ELSEVIER

Diamond and Related Materials 8 (1999) 1033–1038

DIAMOND AND RELATED MATERIALS

Secondary electron emission measurements on synthetic diamond films ☆

H.J. Hopman [a,*], J. Verhoeven [a], P.K. Bachmann [b], H. Wilson [b], Ron Kroon [c]

[a] *FOM Institue for Atomic and Molecular Physics, Kruislaan 407, NL-1098 SJ Amsterdam, The Netherlands*
[b] *Philips Research Laboratories Aachen, Weisshausstrasse 2, D-52066 Aachen, Germany*
[c] *Philips Research Laboratories Eindhoven, Prof. Holstlaan 4, NL-5656 Eindhoven, The Netherlands*

Received 29 August 1998; accepted 1 December 1998

Abstract

During the electron irradiation of synthetic diamond films, three successive regimes are encountered as a function of the electron dose: (1) a reduction of the downward band bending of energy levels at the sample surface because an excess of secondary electrons leaves the sample; (2) the creation of an internal electric field in which secondary electrons drift to the surface, leading to an appreciable increase in the secondary emission and to a linear relation between the primary electron energy and the secondary electron yield; and (3) the desorption of hydrogen terminating the carbon surface bonds. The secondary emission thus decreases to very low values. The rate of decrease of secondary emission is similar for C:H- and C:H:Ba-terminated diamond surfaces.

Keywords: Characterization; Chemisorption; Electron spectroscopy; Synthetic diamond

1. Introduction

One of the remarkable features of properly terminated diamond is its negative electron affinity (NEA), meaning that the vacuum energy level lies below the conduction band minimum [1,2]. This allows electrons moving about in the conduction band to escape unhindered into the vacuum. As such, the application of diamond in electron multipliers, electron emitters [3] and particle/photon detectors [4] is receiving much attention. The advent of chemical vapour deposition techniques for the production of polycrystalline diamond films [5–8] intensified the interest in diamond for such applications. NEA in diamond occurs if the surface dangling bonds of the topmost layer of carbon atoms are terminated by atoms of hydrogen [2,9] or other elements [10–12] which effectively transfer negative charge from the adatom to the substrate.

During the irradiation of a semiconductor with an electron beam, the incident electrons lose energy by creating electron/hole pairs. In the bulk, the secondary electrons thus created slow down by creating additional e/h pairs or by colliding with phonons, and ultimately they pile up at the bottom of the conduction band. As a result, the energy distribution of these secondary electrons should have a peak on the low-energy side, corresponding to the slowed secondary electrons, and a tail extending to high energy. Once the secondary electrons have made the transition from the bulk to the vacuum, their energy distribution $N(E)$ can be measured. In NEA materials, there is no surface barrier and all secondary electrons can escape from the bulk. Therefore, the measured $N(E)$ should have the same general shape as the distribution in the bulk. Indeed, $N(E)$ shows a prominent low-energy peak, the so-called ''quasi-thermal'' peak [1,13,14]. The peak is seen in secondary electron spectroscopy with electron or photon beams as the exciting agents [15]. In positive affinity materials, the surface barrier prevents the emission of low-energy electrons and the quasi-thermal peak is absent. Hence, the very high secondary electron emission of diamond and other NEA materials as compared to positive affinity materials is due to the escape of the low-energy secondary electrons. Moreover, measurement of $N(E)$ and its integral, the secondary electron yield, can be used to monitor changes in the affinity of the material.

The NEA of diamond is related to its surface termination. This introduces the problem of electron-stimulated desorption (ESD) of the adatoms under electron

* Corresponding author. Tel.: +31 20 6081234; Fax: +31 20 6684106.
E-mail address: hopman@amolf.nl. (H.J. Hopman)

☆ Presented at the Diamond '98 Conference, Crete, Greece, 13–18 September, 1998.

0925-9635/99/$ – see front matter
PII: S0925-9635(98)00451-8

bombardment/emission. Experiments have demonstrated the elimination of the NEA as a result of the ESD of hydrogen [16]. Therefore, ESD poses a threat to the applications of diamond mentioned above. The question arises as to whether ESD can be reduced or avoided by the application of elements other than hydrogen, notably alkaline or earth-alkaline elements, as adatoms for the NEA of diamond.

In the present work, electron irradiation studies performed on H- and Ba-terminated polycrystalline diamond films are described. In these studies, the secondary electron yield and energy distribution are monitored. In addition, during irradiation, the current flowing through the sample to ground is also followed as a function of time. This target current reveals charging effects which strongly influence the secondary electron (SE) emission yield. Therefore, as well as the results on ESD, these charging effects are also reported because they should be independent of the method used to produce secondary electrons and will occur in diamond films applied in emitters, detectors or multipliers.

2. Experimental

We studied thin (0.1–2 μm) boron-doped polycrystalline diamond films grown by microwave plasma chemical vapour deposition [17]. Deposition from a hydrogen-rich plasma environment ensured complete hydrogen coverage of the sample surface. After being loaded into the SE emission set-up, the samples were flash-heated to 850 °C, because this results in a higher SE yield [13,14]. Flashing removes additional layers adsorbed during the transport of the sample through the air [9], but leaves the hydrogen coverage intact [2,18]. The characteristics of the samples used in this study are detailed in Table 1. Sample L-474 was boron and nitrogen co-doped and behaved in a highly insulating fashion due to carrier compensation.

The experiments were performed in a UHV system ($p = 4 \times 10^{-10}$ mbar) equipped with a standard four-grid LEED/AES system. The same electron beam was used in all studies. The beam was incident along the normal to the sample surface and the spot size on the target was 1 mm^2.

The energy distribution of the secondary electrons $N(E)$ was obtained by using the LEED system as a retarding field energy analyser. In this measurement, a 50 nA/2.7 keV DC electron beam was used. The current through the sample to ground I_t was measured with a Keithley 610C electrometer. The target support was given a small DC bias potential of -1.6 V to avoid loss of information due to work-function differences between the support and the analyser. In the energy distributions shown below, the electron dose for one $N(E)$ measurement amounts to 0.1 mC cm^{-2}. The emitted electron energy is plotted with respect to the Fermi level. The position of the Fermi level is obtained from that of the "σ peak" in the measured energy spectrum of HOPG graphite, which has an energy of 7.6 eV [19].

Table 1
Overview of polycrystalline CVD diamond films used in this study

Sample	Substrate	Thickness (μm)	B doping (cm^{-3})	N doping (cm^{-3})
P-325	Mo	1.0	10^{20}	–
L-506	Si	0.2	10^{19}	–
L-373	Si	0.15	10^{18}	–
L-474	Si	0.5	10^{20}	10^{20}

A different electrical configuration was used to measure the secondary emission characteristic $\delta(E_p)$, where δ is the coefficient of SE emission, which is defined as the ratio of the total emitted electron current to the incident electron current, and E_p is the impact kinetic energy of the primary electrons on the sample surface. With a constant gun voltage V_b, the beam energy was varied by applying a variable bias potential V_t to the sample holder, i.e. $E_p = -e(V_b - V_t)$. In this way, the primary current I_p is not affected [20]. To reduce the total dose, a pulsed electron beam was used. The target current I_t passed through a pulse amplifier, and was measured by a box-car integrator [21]. In terms of the measured current I_t, we have $\delta(E_p) = 1 - [I_t(eV_b - eV_t)/I_p]$. The primary beam current I_p was measured using a Faraday cup at the target position and/or from the target current with $V_t = +90$ V. The measurement of a $\delta(E_p)$ curve over the full range $0\ \text{eV} < E_p < 1800\ \text{eV}$ with an adequate signal to noise ratio (10 in most cases) required a total dose of 5 nC cm^{-2}. This dose is sufficiently small to avoid charging effects [22]. On repeating the measurement, the same result was obtained.

The deposition of sub-monolayer quantities of Ba was achieved with dispensers from SAES Getters. The dispenser, mounted on a manipulator, could be inserted between the target and the LEED screens for deposition, and could be withdrawn before continuing electron-beam probing of the target surface. The dispenser heater current was adjusted to a value which permitted the deposition of 0.05 ML over 1 min. This time is long compared to the time needed to operate the manipulator. During deposition experiments, which usually took about 2 h, the dispenser heating current was kept at the same value. XPS not being available, and being unwilling to risk the ESD of adatoms by using AES (requiring in our experiment a high dose of 0.1 C cm^{-2}), information on the deposition rate was obtained by following the same procedure with a metallic substrate (polished OFHC copper). On metals, the secondary emission rises to a maximum for 0.3 ± 0.1 ML of Ba (see Ref. [23] and references therein). Below 1 ML, the sticking coefficient

of Ba on Cu is constant [23] and essentially equal to 1. Confirmation of the Ba deposition rate on Cu was obtained from the amplitude of the elastic peak in $N(E)$ when using an 80 eV primary beam. This amplitude saturates at 1 ± 0.2 ML. When measured a few hours after Ba deposition, the maximum SE yield shows a 3% variation over the Cu surface.

A Kaufman ion gun was available for sputter-cleaning targets. In the present case, with the accelerator switched off, a discharge in hydrogen gas was used to provide an in situ source of low-energy atomic hydrogen.

3. Results and interpretation

When irradiating a single spot on a p-type diamond film with an electron beam of $I_p = 100$ nA, three time domains are observed in the target current I_t. In each time domain, I_t shows an exponential time dependence according to $I_t(t) = I_0 \pm I_1 \exp(-t/\tau_c)$, where τ_c is the characteristic time rate of change. The product $I_p\tau_c$ gives a characteristic dose D_c. Because the values of τ_c in the different domains vary by three orders of magnitude, the current is adjusted to reduce measuring times when studying individual domains. Typical D_c values in case of a 1 keV primary beam are:The variation of I_t points to a dose-dependent secondary emission. Only the secondary emission of the irradiated spot appears to be affected. A comparison of the D_c values with the doses needed for measurements shows that the $\delta(E_p)$ curves are not perturbed by the time dependence. Hence, the SE yield measurement correctly probes the state of the target. However, $N(E)$ cannot be determined in the first time domain, and AES cannot be used at all. In the case of p-type samples, the flow of current is unimpeded. The reverse is true for the highly insulating sample L-474 (co-doped with N and B). When switching on the irradiation, the target current decays to 0. The sample behaves as a normal insulator [14]. A positive surface potential regulates the secondary emission to $\delta = 1$.

First time domain	I_t decreases with time	$D_{c1} = 0.2$ mC cm^{-2},
Second time domain	I_t increases with time	$D_{c2} = 2$ mC cm^{-2},
Third time domain	I_t decreases with time	D_{c3} 200 mC cm^{-2}.

3.1. First time domain

In the first time domain, the target current decreases. This is a transient phenomenon which is seen each time the beam is switched on, and also if the off period lasts for periods as short as 1 min. The effect is strongly sample-dependent. After irradiation is terminated, the $\delta(E_p)$ curves are reduced over the whole range by between 0 and 20%. For sample P-325, the effect was studied as a function of E_{p0}, the primary beam energy during irradiation. For each measurement, a different spot on the same target was used. Fig. 1 shows the characteristic time τ_{c1} versus the inverse of δ (determined before irradiation), with E_{p0} as a parameter. The straight line is a linear fit passing through the origin. Fig. 1 shows that the phenomenon is characterised by a constant net quantity of negative charge $Q_1 = I_p\tau_c(\delta - 1)$ leaving the sample, irrespective of the beam energy (or penetration depth). The following explanation is offered. In p-type diamond, there is at the vacuum side a layer of negative charge associated with the downward bending of the energy levels [12,13]. During irradiation, the escaping SEs leave behind their twin holes, and therefore the negative charge will be reduced or become positive. The quantity of charge Q_1 (corresponding to 1 mC cm^{-2}) is much larger than that associated with the downward band bending. So, a dynamic equilibrium is established with a slightly positive surface voltage. On the vacuum side, the lowest-energy SEs are reflected back to the target and the SE emission decreases. Note that the -1.6 V bias of the target support does not modify these events because the combination of a positive surface charge plus its mirror image in the substrate essentially creates a dipole field. Therefore, close to the surface there always exists a potential well for electrons [24]. The transient character of the change in current suggests that the holes which build up the positive surface charge occupy shallow traps and detrap as soon as irradiation is terminated.

3.2. The second time domain

Figs. 2 and 3 demonstrate the increase in the SE yield and the height N_{max} of the quasi-thermal peak in the energy distribution $N(E)$ as a function of dose during irradiation with a 2.7 keV beam. When these data are plotted as a function of the irradiation time, N_{max} and

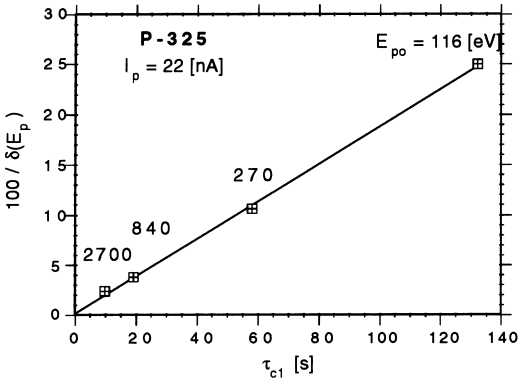

Fig. 1. The characteristic time rate of change τ_{c1} of the current flowing through the sample against the inverse of the coefficient of secondary emission $\delta(E_{p0})$ (determined before irradiation), with the energy of the incident electron beam E_{p0} as a parameter. The straight line is a linear fit passing through the origin.

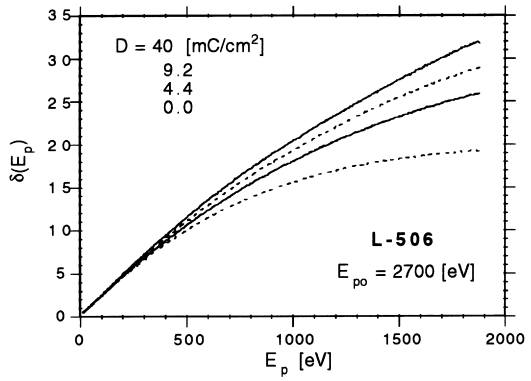

Fig. 2. The monotonic increase in SE emission as a result of low-dose irradiation. The order of the dose values D corresponds to that of the $\delta^* \equiv \delta(E_p = 1.8\ \text{keV})$ values. Primary current: $I_p = 45$ nA. Figs. 2 and 3 are derived from a single sequence of measurements.

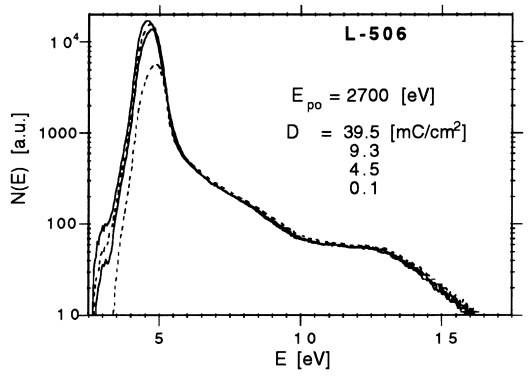

Fig. 3. The monotonic increase of N_{max}, the maximum in the SE distribution function $N(E)$, under low-dose irradiation. The order of the dose values D corresponds to that of the N_{max} values. Note the extension of $N(E)$ to lower values. Further, a shoulder emerges, which is a sign of downward band-bending of the bottom of the conduction band.

$\delta(E_p = 1.8\ \text{keV})$ show the same exponential dependence as the target current, which was recorded in the intervals between these measurements. Note that the δ curve deviates from the usual shape and tends to be linear for $E_p > 500$ eV [14]. This effect is seen more clearly on sample P-325 (see Fig. 4(a)). This phenomenon was studied as a function of the beam energy during irradiation (E_{p0}). For several values of E_{p0}, Fig. 4(b) presents the difference of the δ curves measured after and before irradiation. Note that the highest-energy electrons used (2700 eV) have a penetration depth of $R_p \approx 140$ nm, which is shorter than the thickness of the diamond films in these samples. The sample condition with the high SE yield is stable in UHV on the timescale of weeks.

As shown in Fig. 3, there is no change in $N(E)$ for $E > 5$ eV. As explained in Section 1, this part of $N(E)$ mainly contains SEs which have not had the time to cool down, and therefore they must have been created near the surface. Because under irradiation their escape probability remains constant, the surface is not perturbed for an electron dose of $D < 40\ \text{mC cm}^{-2}$. An additional proof that the increase in the SE yield is not surface-related comes from the fact that the same increase is found after the deposition of Ba onto the surface. Fig. 3 shows that the increase in SE yield is due to a larger number of quasi-thermal SEs. These electrons are created "deep" in the bulk of the sample, and on their way to the surface they cool down. If their number increases, their transport to the surface is more efficient. We hypothesise that during the second time domain, an internal electric field is established. In this field, the SEs drift toward the surface. At birth, the momentum of the SEs has an arbitrary direction. Due to the field, a momentum initially directed into the bulk is turned around and the SEs finally end up at the surface and escape. The field must be homogeneous, because, as Fig. 4(b) proves, irradiation with a $E_{p0} = 430$ eV beam induces a change in the δ curve for $E_p \gg 430$ eV. In agreement with this, the δ curve becomes linear, indicating a constant escape probability of the SEs, independent of the depth of their creation. For the P-325 sample, the derivative $(dE_p/d\delta)$ indicates that 50 eV is expended per emitted SE. As the value found this way is large compared to the e/h pair creation energy of 13 eV, we conclude that the majority of the created SEs recombine, and that a small fraction of about one quarter is able

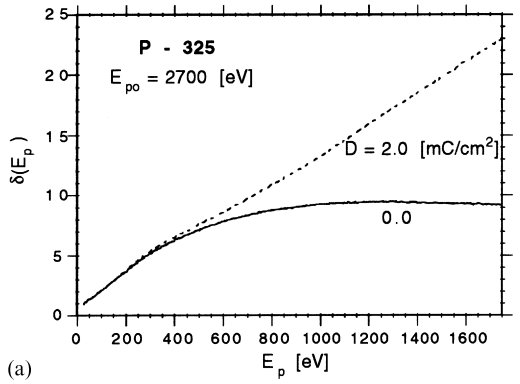

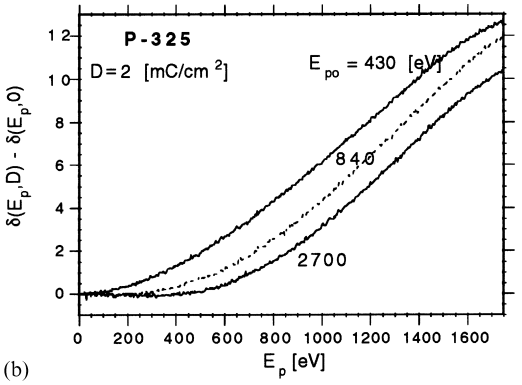

Fig. 4. (a) The increase in the SE yield of sample P-325 under irradiation by an $E_{p0} = 2.7$ keV, $I_p = 45$ nA beam. (b) The difference in the SE yield curves after and before irradiation with a fixed dose of $D = 2\ \text{mC cm}^{-2}$ for several values of E_{p0}.

to escape the sample. An estimate of the magnitude of the electric field F is obtained by demanding that a thermalised SE ($E>0.1$ eV) is slowed down by a distance of $l<100$ nm. This gives $F>10^4$ V cm^{-1}.

Because the electric field is present in the bulk of the sample, it is created by the trapping of electrons, possibly at the interface between the diamond and the substrate. In UHV, the state of the sample after irradiation persists for weeks. So, contrary to the holes, which detrap rapidly, the electrons occupy deep traps.

The co-doped sample L-474 has a maximum SE yield of $\delta_{max}=7.1\pm0.1$ and does not show the quasi-thermal peak in $N(E)$. A small irradiation dose (50 mC cm^{-2}) leads to a 20% decrease in δ_{max} which is recovered on the timescale of a few days.

3.3. The third time domain

Irradiation up to doses of 1 C cm^{-2} leads to the loss of NEA, resulting in a small SE yield (see Figs. 5 and 6). The loss of NEA is due to the electron-stimulated desorption of hydrogen [13]. This is proved by a complete recovery of the SE yield to the original value of the flashed sample after exposure to atomic hydrogen. High-dose irradiation leads to a modification of the surface, and accordingly there is a change in $N(E)$ for $E>5$ eV (see Fig. 6), in contrast to Fig. 3. Data with the characteristic doses D_{c2} and D_{c3} in the second and third time domains are collected in Table 2.

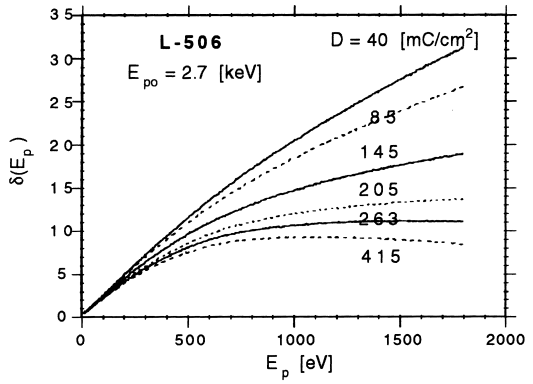

Fig. 5. Monotonic decrease in SE emission under high-dose irradiation. Primary current: $I_p=500$ nA. The order of the dose values D corresponds to that of the $\delta^*\equiv\delta(E_p=1.8\text{ keV})$ values.

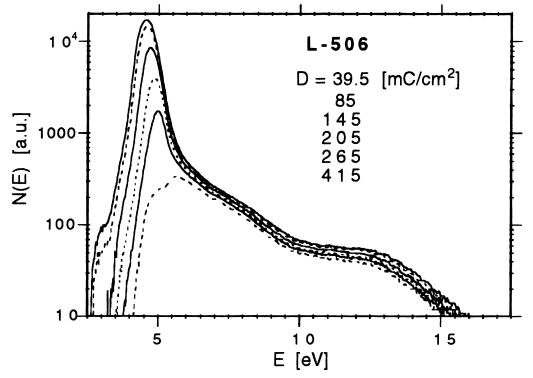

Fig. 6. Monotonic decrease of N_{max} under high-dose irradiation. The order of the dose values D corresponds to that of the N_{max} values. Figs. 5 and 6 are derived from a single sequence of measurements.

3.4. Ba deposition

Comparing the SE yields measured during the deposition of Ba on Cu or on diamond, it is found that on diamond the peak in the yield occurs at a slightly smaller number of deposition steps. Assuming equal sticking coeffcients, the yield is maximal after the deposition of 0.25 ML. Two time-dependent phenomena accompany Ba deposition: (1) 2 h directly after the deposition of about 0.5 ML, $\delta^*\equiv\delta(E_p=1.8\text{ keV})$ increases linearly with time until saturating at about double its value: this saturation value is higher that the maximum observed during deposition; and (2) while remaining in UHV, δ^* decreases on a timescale of 100 h. To study the linear increase of δ^* after Ba deposition, the experiment was repeated without flashing the sample. The same sequence of phenomena was observed. This suggests a high room-temperature mobility of Ba, as also observed on metallic substrates [23]. This suggestion is supported by the observation that the amplitude of the elastic peak in $N(E)$ recovers the low-coverage value. Also, the final SE yield is fairly homogeneous (10%) over the sample surface. On the other hand, AES directly after deposition shows the presence of sub-ML quantities of oxygen, despite a background pressure of 4×10^{-10} mbar. Although oxygen deposition could have been induced by AES, the co-deposition of oxygen with the Ba cannot be excluded. One indication of a change in surface properties is the variation in amplitude of $N(E)$ over the whole range 0 eV$<E<$17.5 eV (contrary to what is observed in Fig. 3). Therefore, directly after Ba deposition, there is a redistribution of Ba over the surface, and possibly a rearrangement of Ba and O positions in the adlayer.

Table 2
Characteristic doses D_{c2} (mC cm^{-2}) for the increase in SE emission under irradiation and D_{c3} (mC cm^{-2}) for the subsequent decrease in SE yield due to hydrogen desorption (second and third time domains). Also presented are the values of $\delta^*\equiv\delta(E_p=1.8\text{ keV})$ of the sample after flashing (mean value over nine points; in the case of L-373 a week after the deposition of Ba), low-dose irradiation and high-dose irradiation (value of the irradiated point)

Sample	Flashed	Low dose irradiation		High dose irradiation	
	$\langle\delta^*\rangle$	D_{c2}	δ^*	D_{c3}	δ^*
P-325	25.2±1.8	20	32	250	15
L-506	21.0±4.0	3.4	31	50	9.3
Ba/L-373	13.3±0.3	3.3	18	250	6.5

The area-averaged values $\langle\delta^*\rangle$ observed a few hours after deposition, are $\langle\delta^*\rangle = 57 \pm 6$ for sample L-506, and $\langle\delta^*\rangle = 20.0 \pm 1.0$ for sample L-373 (coming from 8.1 ± 1.0). The irradiated spots on the samples, from which H had been desorbed before Ba deposition, acquire the same SE yield as other regions which retained their H termination. When, after deposition of Ba, sample L-506 was flashed to 900 °C, it still had $\langle\delta^*\rangle = 30 \pm 4$. As a result of Ba deposition, the work function, as measured from the shift of $N(E)$, decreased by 1.6 V.

The result of small- and high-dose irradiation of the bariated sample is shown in Fig. 7. It shows the same behaviour as was found on L-506 (see Figs. 2 and 5). The irradiation took place six days after Ba deposition, and in this period $\langle\delta^*\rangle$ decreased from 20.0 ± 1.0 to 13.3 ± 0.3. Table 2 shows that the characteristic doses for bariated or hydrogen-terminated samples are similar. After irradiation, the Auger spectra indicate similar quantities of Ba at the surface (but more oxygen). Therefore, the decrease in the SE yield is attributed to the desorption of hydrogen.

4. Conclusion

Thanks to the very different timescales in the case of diamond for the trapping of holes and electrons or the desorption of surface hydrogen, these three processes can be followed unperturbed in the variation of the current transmitted through a sample under irradiation.

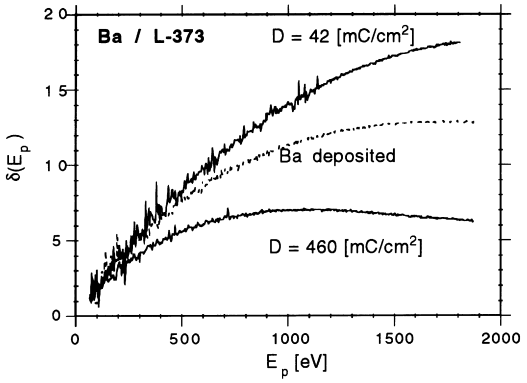

Fig. 7. The phenomena shown in Figs. 2 and 5 also occur on a sample covered by 0.25 ML of Ba. Shown are the yield curves for the bariated sample, and after low- and after high-dose irradiation.

Acknowledgement

The authors thank Mr. H. Zeijlemaker for his enthusiasm and skilful assistance in solving problems.

References

[1] F.J. Himpsel, J.A. Knapp, J.A. VanVechten, D.E. Eastman, Phys. Rev. B 20 (1979) 624.
[2] B.B. Pate, Surf. Sci. 165 (1986) 83.
[3] M.W. Geis, N.N. Efremov, K.E. Krohn, J.C. Twichell, T.M. Lyszcarz, R. Kalish, J.A. Greer, M.D. Tabat, Nature 393 (1998) 431.
[4] R.D. McKeag, R.D. Marshall, B. Baral, S.M. Chan, R.B. Jackman, Diamond Relat. Mater. 6 (1997) 374.
[5] B.V. Spitsyn, L.L. Bouilov, B.V. Derjaguin, J. Crystal Growth 52 (1981) 219.
[6] S. Matsumoto, Y. Sato, M. Kamo, N. Setaka, Jpn. J. Appl. Phys. 21 (1982) L183.
[7] M. Kamo, Y. Sato, S. Matsumoto, N. Setaka, J. Crystal Growth 62 (1983) 642.
[8] P.K. Bachmann, W. v. Enckefort, Diamond Relat. Mater. 1 (1992) 1021.
[9] J. van der Weide, Z. Zhang, P.K. Baumann, M.G. Wensell, J. Bernholc, R.J. Nemanich, Phys. Rev. B 50 (1994) 5803.
[10] R.J. Nemanich, P.K. Baumann, M.C. Benjamin, S.P. Bozeman, B.L. Ward, in: A. Paoletti, A. Tucciarone (Eds.), The Physics of Diamond, IOS Press, 1997.
[11] J.E. Yater, A. Shih, R. Abrams, Phys. Rev. B 56 (1997) R4410.
[12] L. Diederich, O.M. Küttel, P. Aebi, E. Maillard, R. Fasel, L. Schlappbach, Diamond Relat. Mater. 7 (1998) 660.
[13] I.L. Krainsky, V.M. Asnin, G.T. Mearini, J.A. Dayton, Phys. Rev. B 53 (1996) R7650.
[14] A. Shih, J. Yater, P. Pehrsson, J. Butler, C. Hor, R. Abrams, J. Appl. Phys. 82 (1997) 1860.
[15] T.P. Humphreys, R.E. Thomas, D.P. Malta, J.B. Posthill, M.J. Mantini, R.A. Rudder, G.C. Hudson, R.J. Markunas, C. Pettenkofer, Appl. Phys. Lett. 70 (1997) 1257.
[16] R.E. Thomas, T.P. Humphreys, C. Pettenkofer, D.P. Malta, J.B. Posthill, M.J. Mantini, R.A. Rudder, G.C. Hudson, R.J. Markunas, Mater. Res. Soc. Symp. Proc. 416 (1996) 263.
[17] P.K. Bachmann, W. Eberhardt, B. Kessler, H. Lade, K. Radermacher, D.U. Wiecher, H. Wilson, Diamond Relat. Mater. 5 (1996) 1378.
[18] B.D. Thoms, P.E. Pehrsson, J.E. Butler, J. Appl. Phys. 75 (1994) 1804.
[19] P. Oelhafen, J.L. Freeouf, J. Vac. Sci. Technol. A 1 (1983) 96.
[20] V.E. Henrich, Rev. Sci. Instrum. 44 (1973) 456.
[21] H.J. Hopman, J. Verhoeven, J.J. Scholtz, R. Fastenau, Appl. Surf. Sci. 111 (1997) 270.
[22] I.L. Krainsky, G.G. Lesny, Rev. Sci. Instrum. 69 (1998) 1916.
[23] U. van Slooten, W.R. Koppers, A. Bot, H.M. van Pinxteren, A.M.C. Motinho, J.W.M. Frenken, A.W. Kleyn, J. Phys. Condens. Matter 5 (1993) 5411.
[24] J.J. Scholtz, R.W.A. Schmitz, B.H.W. Hendriks, S.T. de Zwart, Appl. Surf. Sci. 111 (1997) 259.